Electronic Supplementary Material (ESI) for ChemComm.
This journal is © The Royal Society of Chemistry 2017

Manipulating and quantifying spin state in solution as a function of pressure and temperature

Ross W. Hogue,[†] Christopher P. Lepper,[‡] Geoffrey B. Jameson,[‡] Sally Brooker*[†]*

[†]Department of Chemistry and MacDiarmid Institute for Advanced Materials and Nanotechnology, University of Otago, PO Box 56, Dunedin 9054, New Zealand. Email: sbrooker@chemistry.otago.ac.nz

[‡]Chemistry – Institute of Fundamental Sciences and MacDiarmid Institute for Advanced Materials and Nanotechnology, Massey University, Private Bag 11 222, Palmerston North 4442, New Zealand.

ELECTRONIC SUPPORTING INFORMATION

Synthetic experimental details:

TGA was recorded on a TA instruments Q50 with the samples in a platinum pan heated at 20°C min^{-1}. Nitrogen gas flow was set to 40 mL min^{-1} over the balance and 60 mL min^{-1} over the sample. Microanalysis was performed by the Campbell Microanalytical Laboratory at the University of Otago. 4-substituted-3,5-bis{[(2-pyridylmethyl)-sulfanyl]methyl}-4H-1,2,4-triazole (**PSRT**) ligands: **PSPhT**, **PS^{Me}PhT**, and **PS^{i}BuT**; and the di-iron [Fe$^{II}_2$(**PSRT**)$_2$](BF$_4$)$_4$·solvent complexes were prepared as reported.[1] Dry THF was obtained from a Pure Solv MD-6 Solvent Purification System. All other chemicals were purchased from commercial suppliers and were used as received.

[Zn$^{II}_2$(**PSPhT**)$_2$](BF$_4$)$_4$·1½THF. To a clear yellow solution of **PSPhT** (63.8 mg, 0.152 mmol) in 10 mL dry THF was added a solution of Zn(BF$_4$)$_2$·H$_2$O (36.3 mg, 0.152 mmol) in 5 mL dry THF. Immediately a white precipitate appeared, which was stirred overnight. Filtration of the white powder and drying in vacuo yielded [Zn$^{II}_2$(**PSPhT**)$_2$](BF$_4$)$_4$·1½THF (45.3 mg, 0.031 mmol, 41%). Anal. calcd for [Zn$^{II}_2$(**PSPhT**)$_2$](BF$_4$)$_4$·1½THF: C 42.14, H 3.82, N 9.83, S 9.00%; found: C 42.23, H 4.03, N 9.64, S 8.86%. Slow diethyl ether vapour diffusion into a MeCN solution of the product produced several colourless clusters of crystalline material, one of which could be cut to yield a single block shaped crystal of [Zn$_2$(**PSPhT**)$_2$](BF$_4$)$_4$·2MeCN suitable for X-ray diffraction (see later, Figure S20, Table S13).

[Zn$^{II}_2$(**PS^{Me}PhT**)$_2$](BF$_4$)$_4$·⅓THF. To a clear yellow solution of **PS^{Me}PhT** (41.4 mg, 0.0955 mmol) in 7 mL dry THF was added a solution of Zn(BF$_4$)$_2$·H$_2$O (23 mg, 0.096 mmol) in 3 mL dry THF. After 30 seconds a white precipitate appeared, which was stirred overnight. Filtration of the white powder and drying in vacuo yielded [Zn$^{II}_2$(**PS^{Me}PhT**)$_2$](BF$_4$)$_4$·⅓THF (28.1 mg, 0.0205 mmol, 43%). Anal. calcd for [Zn$^{II}_2$(**PS^{Me}PhT**)$_2$](BF$_4$)$_4$·⅓THF: C 41.52, H 3.58, N 10.23, S 9.37%; found: C 41.85, H 3.79, N 10.45, S 9.47%. TGA: Calcd. 1.8% found 1.7%.

[Zn$^{II}_2$(**PS^{i}BuT**)$_2$](BF$_4$)$_4$·THF. To a clear yellow solution of **PS^{i}BuT** (67.7 mg, 0.169 mmol) in 5 mL dry THF was added a solution of Zn(BF$_4$)$_2$·H$_2$O (40 mg, 0.17 mmol) in 5 mL dry THF under an N_2 atmosphere. Immediately a white precipitate appeared, which was stirred overnight. Filtration of the white powder under a stream of N_2 and drying in vacuo yielded [Zn$^{II}_2$(**PS^{i}BuT**)$_2$](BF$_4$)$_4$·THF (65 mg, 0.048 mmol, 57%). Anal. calcd for [Zn$^{II}_2$(**PS^{i}BuT**)$_2$](BF$_4$)$_4$·THF: C 39.17, H 4.33, N 10.38, S 9.50%; found: C 38.67, H 4.42, N 10.64, S 9.29%. TGA: Calcd. 5.3% found 5.4%.

High Pressure NMR instrument details:

^{1}H NMR spectra were recorded at Massey University, Palmerston North, New Zealand on a Bruker Avance 500 MHz NMR spectrometer. High-pressure experiments were conducted using a custom-built on-line high pressure set-up:[2] this consists of a zirconia NMR tube (5 mm outer diameter, 3 mm inner diameter, Daedalus Innovations) attached to an aluminum manifold, connected to a remote handpump via a stainless steel tube containing the pressurizing fluid (low viscosity paraffin oil). The studied acetonitrile solutions are pressurized via immiscible paraffin oil to any value between 0.1 MPa (handpump open to atmosphere) and 240 MPa to an accuracy of 1 MPa. The temperature controller employed has a lower limit of 278 K, and spectra were recorded at a maximum of 313 K, above which temperature the paraffin oil appears to become slightly miscible with acetonitrile.

Solution preparation:

For each iron complex, variable-pressure spectra at 283-313 K were recorded on the same solution, which was separately prepared, and at a different concentration to that used for measurements at 278 K. Diamagnetic corrections to Fe(II) data at 278 K were made using the Zn(II) complex of the same

ligand as the diamagnetic correction. Each of the three Zn(II) complexes was observed to behave almost identically, with respect to CD_2HCN position, with a) varying pressure at 278 K, and b) varying temperature at atmospheric pressure (Figures S4 and S5). Therefore diamagnetic corrections to data of each Fe(II) complex at 283-313 K were made using only $[Zn^{II}_2(\mathbf{PS^{i}BuT})_2](BF_4)_4$. Samples were prepared by dissolving an accurately weighed amount of either Fe(II) or Zn(II) complex into 630 or 650 µL of CD_3CN. Fe(II) solutions were prepared to a concentration which was as close as possible to the Zn(II) complex solution to be used as the diamagnetic correction for that particular data set, as described in table S1.

Table S1. Concentration of Fe(II) complex solutions, and diamagnetic reference solutions and concentrations used.

Fe(II) complex	Data set	Concentration	Diamagnetic reference used; concentration
$[Fe^{II}_2(\mathbf{PSPhT})_2](BF_4)_4{\cdot}CH_3CN$	278 K	10.60 mmol L^{-1}	$[Zn^{II}_2(\mathbf{PSPhT})_2](BF_4)_4{\cdot}1½THF$; 10.55 mmol L^{-1}
	283 – 313 K	11.23 mmol L^{-1}	$[Zn^{II}_2(\mathbf{PS^{i}BuT})_2](BF_4)_4{\cdot}THF$; 11.22 mmol L^{-1}
$[Fe^{II}_2(\mathbf{PS^{Me}PhT})_2](BF_4)_4$	278 K	8.77 mmol L^{-1}	$[Zn^{II}_2(\mathbf{PS^{Me}PhT})_2](BF_4)_4{\cdot}⅓THF$; 8.79 mmol L^{-1}
	283 – 313 K	11.19 mmol L^{-1}	$[Zn^{II}_2(\mathbf{PS^{i}BuT})_2](BF_4)_4{\cdot}THF$; 11.22 mmol L^{-1}
$[Fe^{II}_2(\mathbf{PS^{i}BuT})_2](BF_4)_4{\cdot}½H_2O$	278 K	11.22 mmol L^{-1}	$[Zn^{II}_2(\mathbf{PS^{i}BuT})_2](BF_4)_4{\cdot}THF$; 11.22 mmol L^{-1}
	283 – 313 K	11.22 mmol L^{-1}	$[Zn^{II}_2(\mathbf{PS^{i}BuT})_2](BF_4)_4{\cdot}THF$; 11.22 mmol L^{-1}

Data Collection Procedure:

Each data set was collected as a variable pressure sweep with a fixed temperature. The solution was pressurized to 240 MPa (behind a blast shield), then inserted into the NMR instrument, and then allowed to equilibrate to the set temperature during the 20 minutes following instrument temperature stabilization. The acetonitrile lock signal was obtained, shimming and tuning of the magnet were performed, before the lock was turned off. Spectra were then recorded in decreasing pressure intervals of 30 MPa until 0.1 MPa (pressure cell open to atmosphere), with wait times of at least 5 minutes between spectra to allow any thermal effects of changing pressure to dissipate. In the case of data recorded at 283 K – 313 K, the same solution was used. Here the 283 K pressure sweep was recorded first, then the pressure cell was removed from the instrument to be repressurized to 240 MPa before being reinserted to the instrument and allowed to equilibrate to 293 K. Lock, shims, tuning and lock-off were repeated before spectra were recorded with decreasing pressure. Spectra at 303 K, and 313 K were subsequently recorded by this procedure. In the case of the pressure sweep measurements of the three Zn(II) complexes at 278 K, after recording the 0.1 MPa spectrum, spectra were also recorded (at 0.1 MPa) at 283 K, 293 K, 303 K, and 313 K. Spectra of the Fe(II) complexes are presented in Figures S1-S3.

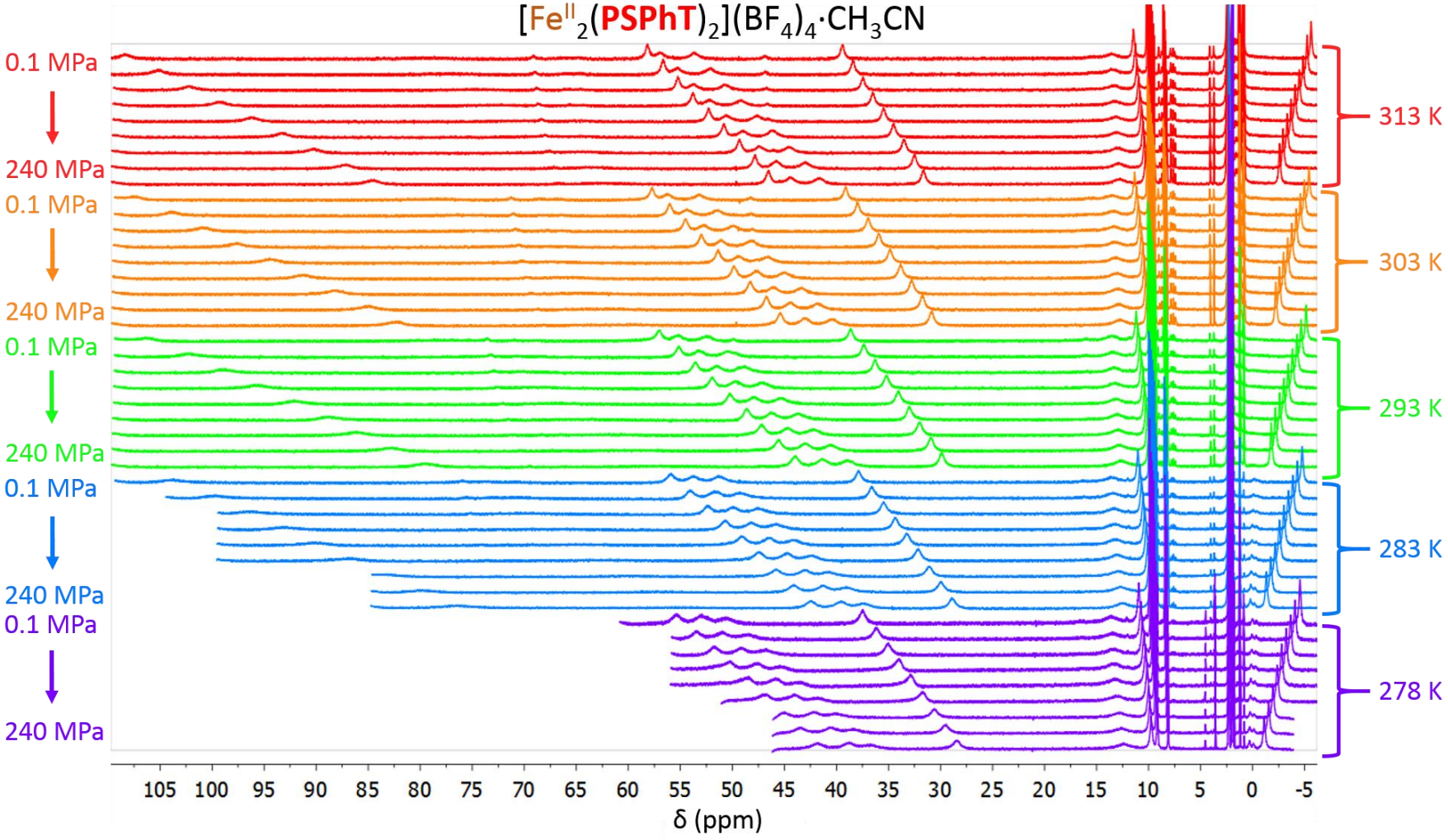

Figure S1. ^{1}H NMR spectra of [Fe$^{II}_2$(**PSPhT**)$_2$](BF$_4$)$_4$·CH$_3$CN in CD$_3$CN at all investigated pressures/temperatures. Spectra are coloured according to temperature, each temperature series is presented from top to bottom from atmospheric pressure to 240 MPa increasing in pressure by 30 MPa.

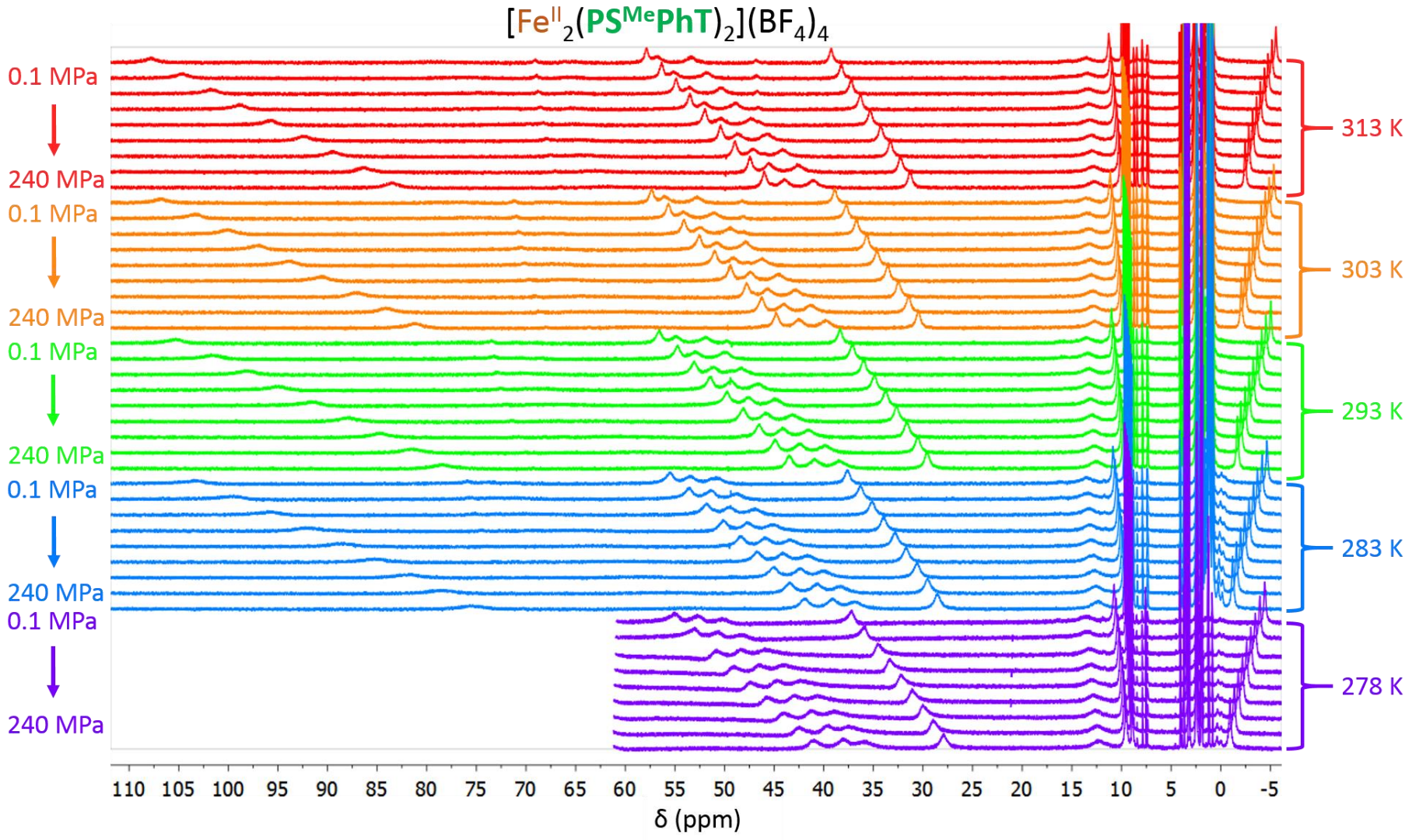

Figure S2. ^{1}H NMR spectra of [Fe$^{II}_2$(PS^{Me}PhT)$_2$](BF$_4$)$_4$ in CD_3CN at all investigated pressures/temperatures. Spectra are coloured according to temperature, each temperature series is presented from top to bottom from atmospheric pressure to 240 MPa increasing in pressure by 30 MPa.

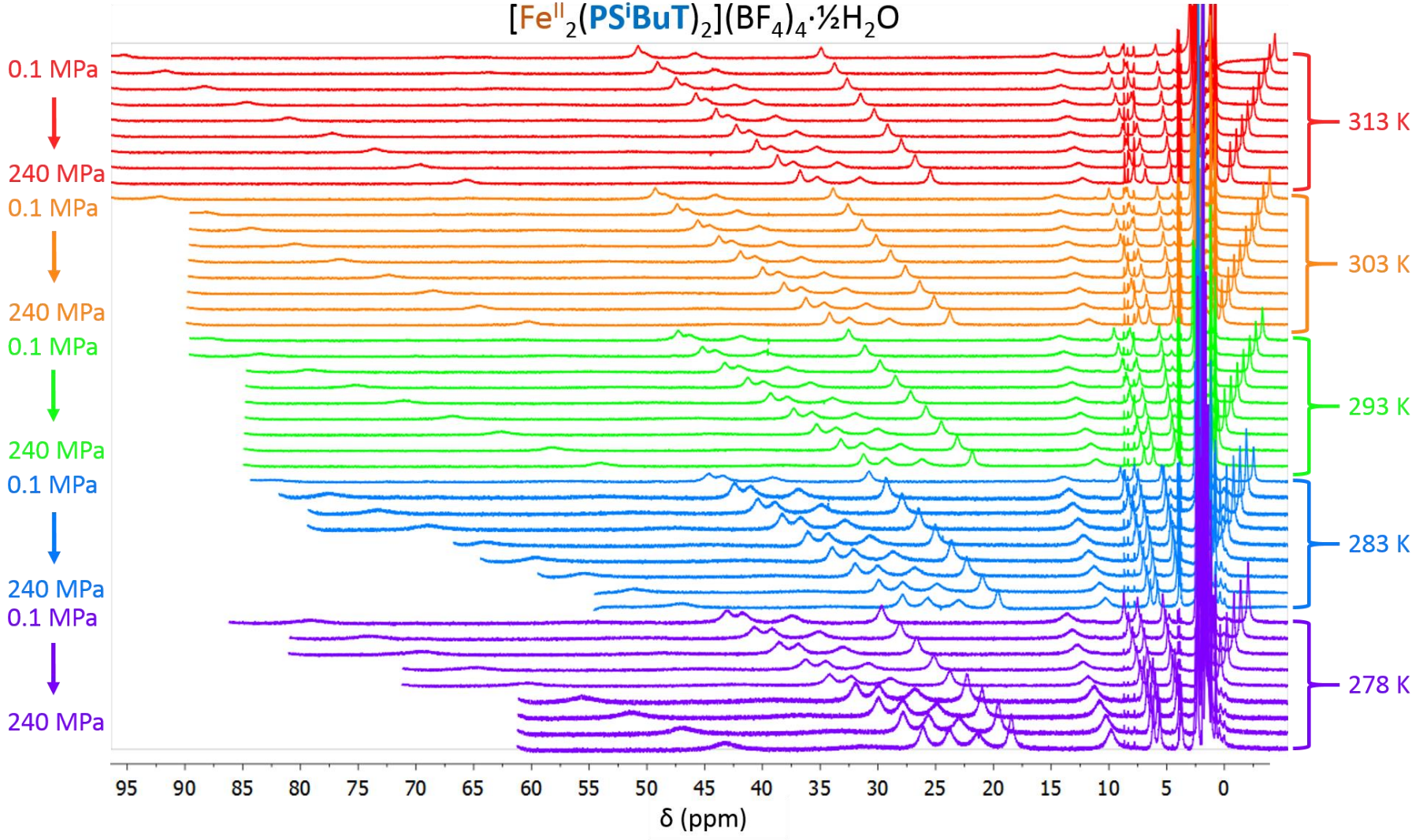

Figure S3. ^{1}H NMR spectra of [Fe$^{II}_2$(PS^{i}BuT)$_2$](BF$_4$)$_4$·½H$_2$O in CD$_3$CN at all investigated pressures/temperatures. Spectra are coloured according to temperature, each temperature series is presented from top to bottom from atmospheric pressure to 240 MPa increasing in pressure by 30 MPa.

Treatment of data

Time Corrections

CD_2HCN peak positions (Hz) were first corrected for the time-dependent drift in CD_2HCN signal with lock-off due to the magnet strength decreasing slowly after tuning. Data were corrected relative to the first recorded spectra of that temperature (240 MPa in each case), by the linear relationship of signal position changing by -0.0005927 Hz s^{-1}. This relationship was determined by monitoring the position of the CD_2HCN signal in pure CD_3CN over 40 minutes (one pressure sweep at a given temperature typically takes 1 hour, so this relationship was extended by at most 20 minutes. The time correction is at most ≈2 Hz applied to the last recorded spectra of that data set which differed in CD_2HCN position by ≈200 Hz from the t = 0 spectrum).

Diamagnetic Zn(II) reference solutions

The diamagnetic Zn(II) analogues of the Fe(II) complexes were prepared after it was discovered that the p-T behaviour of the ligand-only ^{1}H NMR signal of CD_2HCN was significantly different to that of pure CD_2HCN (Figure S4). For the Zn(II) complex solutions at 278 K, after having applied the time corrections to the spectra, CD_2HCN signal positions were recorded as the change in signal position relative to that in the spectrum at atmospheric pressure (0.1 MPa). This quantity, $\Delta\Delta f$(Zn) in Hz (Table S2, Figure S4), is used as the diamagnetic correction of pressure-dependent CD_2HCN signal position variation to be applied to the spectra of the corresponding Fe(II) complex solutions at 278 K as a point by point correction. The temperature dependence of the CD_2HCN signal position in the Zn(II) solutions was investigated, here $\Delta\Delta f$(Zn) is relative to 278 K, 0.1 MPa (Table S3, Figure S5). The diamagnetic correction applied to spectra of Fe(II) solutions between 283 – 313 K was in each case $[Zn^{II}_2(\mathbf{PS^iBuT})_2](BF_4)_4\cdot$THF (11.22 mmol L^{-1}). For this $\Delta\Delta f$(Zn) of each data point is reported as relative to the 0.1 MPa spectrum of the same temperature (Table S4).

The difference in χ_M or $\chi_M T$ values derived using either the Zn(II) analogues of the Fe(II) complexes or the free ligand as the diamagnetic reference are within error at all pressures (Table S2 and Figure S4); using free ligand as the diamagnetic reference is the usual practice in Evans' method susceptibility measurements, and is indeed satisfactory here. For this study, as a complete background correction data set was collected on $[Zn^{II}_2(\mathbf{PS^iBuT})_2](BF_4)_4\cdot$THF only, this was used as the diamagnetic reference.

Table S2. $\Delta\Delta f$(Zn) values, in Hz, at 278 K and variable pressures for the solutions of $[Zn^{II}_2(\mathbf{PSPhT})_2](BF_4)_4\cdot1½$THF (10.55 mmol L^{-1}), $[Zn^{II}_2(\mathbf{PS^{Me}PhT})_2](BF_4)_4\cdot⅓$THF (8.79 mmol L^{-1}), $[Zn^{II}_2(\mathbf{PS^iBuT})_2](BF_4)_4\cdot$THF (11.22 mmol L^{-1}), and free $\mathbf{PS^{Me}PhT}$ ligand (9.80 mmol L^{-1}).

Pressure (MPa)	$[Zn^{II}_2(\mathbf{PSPhT})_2](BF_4)_4\cdot1½$THF (10.55 mM)	$[Zn^{II}_2(\mathbf{PS^{Me}PhT})_2](BF_4)_4\cdot⅓$THF (8.79 mM)	$[Zn^{II}_2(\mathbf{PS^iBuT})_2](BF_4)_4\cdot$THF (11.22 mM)	$\mathbf{PS^{Me}PhT}$ ligand (9.80 mM)
240	-72.45	-73.43	-70.88	-67.26
210	-67.95	-68.37	-66.34	-65.43
180	-61.46	-61.84	-60.23	-59.27
150	-54.92	-55.19	-53.51	-52.98
120	-46.81	-46.92	-46.10	-44.62
90	-38.08	-38.06	-37.71	-36.55
60	-27.67	-27.73	-27.80	-27.33
30	-16.14	-16.36	-16.40	-16.28
0.1	0	0	0	0

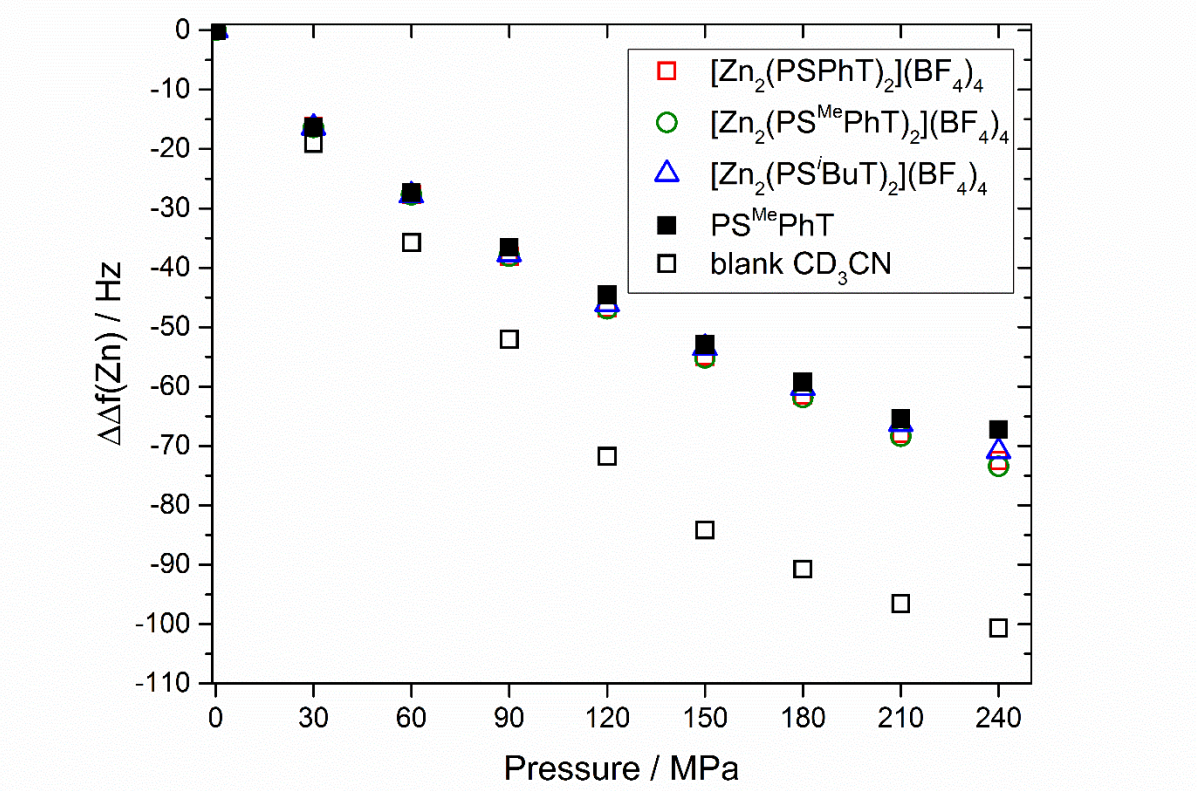

Figure S4. ΔΔ*f*(Zn) values, in Hz, vs pressure at 278 K for the solutions of $[Zn^{II}_2(\mathbf{PSPhT})_2](BF_4)_4\cdot 1\frac{1}{2}THF$ (10.55 mmol L^{-1}), $[Zn^{II}_2(\mathbf{PS^{Me}PhT})_2](BF_4)_4\cdot \frac{1}{3}THF$ (8.79 mmol L^{-1}), $[Zn^{II}_2(\mathbf{PS^{i}BuT})_2](BF_4)_4\cdot THF$ (11.22 mmol L^{-1}) in CD_3CN. Also shown are the change in frequency, in Hz, of the CD_2HCN signal at variable pressures, relative to 0.1 MPa, all at 278 K for a solution of free **PS^{Me}PhT** ligand in CD_3CN (9.80 mmol L^{-1}) and blank CD_3CN; note these two solutions were not used as diamagnetic references.

Table S3. ΔΔ*f*(Zn) values, in Hz, at 0.1 MPa and variable temperatures for the solutions of $[Zn^{II}_2(\mathbf{PSPhT})_2](BF_4)_4\cdot 1\frac{1}{2}THF$ (10.55 mmol L^{-1}), $[Zn^{II}_2(\mathbf{PS^{Me}PhT})_2](BF_4)_4\cdot \frac{1}{3}THF$ (8.79 mmol L^{-1}), and $[Zn^{II}_2(\mathbf{PS^{i}BuT})_2](BF_4)_4\cdot THF$ (11.22 mmol L^{-1}).

Temperature (K)	**$[Zn^{II}_2(PSPhT)_2](BF_4)_4\cdot 1\frac{1}{2}THF$ (10.55 mmol L^{-1})**	**$[Zn^{II}_2(PS^{Me}PhT)_2](BF_4)_4\cdot \frac{1}{3}THF$ (8.79 mmol L^{-1})**	**$[Zn^{II}_2(PS^{i}BuT)_2](BF_4)_4\cdot THF$ (11.22 mmol L^{-1})**
278	0	0	0
283	6.055	6.60	6.34
293	18.87	19.75	18.69
303	32.10	33.39	31.27
313	45.58	45.49	44.78

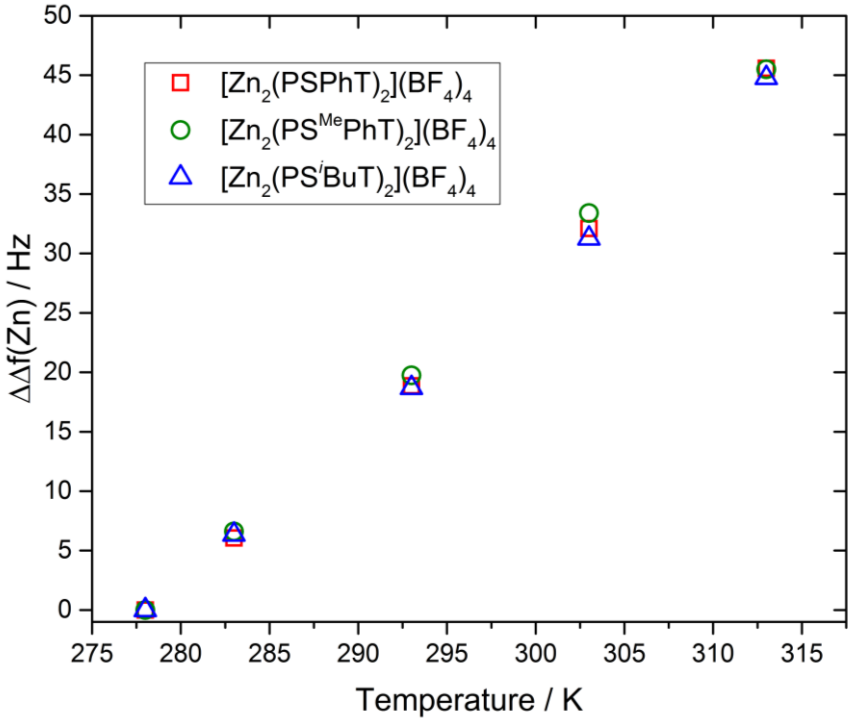

Figure S5. ΔΔ*f*(Zn) values, in Hz, vs temperature at 0.1 MPa for the solutions of $[Zn^{II}_2(\mathbf{PSPhT})_2](BF_4)_4 \cdot 1\frac{1}{2}THF$ (10.55 mmol L^{-1}), $[Zn^{II}_2(\mathbf{PS^{Me}PhT})_2](BF_4)_4 \cdot \frac{1}{3}THF$ (8.79 mmol L^{-1}), and $[Zn^{II}_2(\mathbf{PS^{i}BuT})_2](BF_4)_4 \cdot THF$ (11.22 mmol L^{-1}).

Table S4. ΔΔ*f*(Zn), in Hz, at various pressures and temperatures of $[Zn^{II}_2(\mathbf{PS^{i}BuT})_2](BF_4)_4 \cdot THF$ (11.22 mmol L^{-1}).

Pressure (MPa)	ΔΔ*f*(Zn) / Hz of $[Zn^{II}_2(\mathbf{PS^{i}BuT})_2](BF_4)_4 \cdot THF$ (11.22 mmol L^{-1})			
	283 K	293 K	303 K	313 K
240	-74.27	-79.60	-86.19	-91.96
210	-68.86	-74.48	-79.35	-84.72
180	-61.94	-67.23	-71.72	-76.80
150	-54.63	-59.69	-63.55	-68.16
120	-46.36	-51.03	-54.56	-58.43
90	-36.93	-40.72	-44.02	-47.08
60	-26.74	-29.22	-31.91	-34.55
30	-15.01	-16.76	-18.27	-19.87
0.1	0	0	0	0

Paramagnetic Fe(II) solutions

First, time corrections were applied to the spectra as detailed above. CD_2HCN signal positions were then interpreted as a change in position relative to that of the 0.1 MPa spectrum of the same temperature, ΔΔ*f*(Fe) in Hz. These are then corrected for the change in CD_2HCN signal position due to pressure/temperature variation without any change in spin state; this is done by subtracting ΔΔ*f*(Zn) for each particular pressure/temperature point (using the diamagnetic reference solution as outlined in Table S1). This gives ΔΔ*f*(SCO), the change in CD_2HCN signal position due to a change in spin state; ΔΔ*f*(SCO) = ΔΔ*f*(Fe) – ΔΔ*f*(Zn). The resulting ΔΔ*f*(SCO) values, in Hz, are reported in Tables S5-S7.

Table S5. ΔΔ*f*(SCO), in Hz, at various pressures and temperatures of $[Fe^{II}_2(PSPhT)_2](BF_4)_4 \cdot CH_3CN$.

Pressure (MPa)	ΔΔ*f*(SCO) / Hz of $[Fe^{II}_2(PSPhT)_2](BF_4)_4 \cdot CH_3CN$				
	278 K[a]	283 K[b]	293 K[b]	303 K[b]	313 K[b]
240	-96.16	-79.83	-82.62	-69.03	-54.21
210	-84.80	-67.17	-68.73	-59.38	-44.84
180	-75.14	-55.74	-56.23	-48.13	-34.32
150	-66.31	-44.96	-44.44	-36.86	-24.81
120	-57.80	-34.31	-33.53	-26.71	-16.57
90	-42.38	-24.52	-23.66	-17.38	-9.31
60	-25.03	-14.70	-14.26	-10.32	-4.27
30	-12.17	-6.46	-6.39	-4.09	-0.60
0.1	0.00	0.00	0.00	0.00	0.00

[a]10.60 mmol L^{-1}. [b]11.23 mmol L^{-1}

Table S6. ΔΔ*f*(SCO), in Hz, at various pressures and temperatures of $[Fe^{II}_2(PS^{Me}PhT)_2](BF_4)_4$.

Pressure (MPa)	ΔΔ*f*(SCO) / Hz of $[Fe^{II}_2(PS^{Me}PhT)_2](BF_4)_4$				
	278 K[a]	283 K[b]	293 K[b]	303 K[b]	313 K[b]
240	-84.00	-90.43	-80.74	-68.82	-59.33
210	-74.47	-78.90	-69.27	-58.46	-46.59
180	-66.55	-66.63	-56.79	-47.06	-36.25
150	-58.46	-54.46	-45.41	-36.56	-27.31
120	-51.52	-42.46	-34.74	-26.38	-18.39
90	-43.54	-29.43	-24.56	-17.61	-11.47
60	-24.37	-20.39	-15.67	-9.95	-6.59
30	-9.82	-9.87	-7.20	-3.81	-1.81
0.1	0	0	0	0	0

[a]8.77 mmol L^{-1}. [b]11.19 mmol L^{-1}

Table S7. ΔΔ*f*(SCO), in Hz, at various pressures and temperatures of $[Fe^{II}_2(PS^{i}BuT)_2](BF_4)_4 \cdot ½H_2O$.

Pressure (MPa)	ΔΔ*f*(SCO) / Hz of $[Fe^{II}_2(PS^{i}BuT)_2](BF_4)_4 \cdot ½H_2O$				
	278 K[a]	283 K[b]	293 K[b]	303 K[b]	313 K[b]
240	-131.24	-116.13	-105.85	-88.48	-71.32
210	-117.85	-98.98	-89.41	-72.79	-56.25
180	-101.65	-83.13	-72.94	-58.98	-43.52
150	-87.15	-68.25	-58.18	-45.49	-32.59
120	-71.24	-53.15	-44.09	-32.86	-22.43
90	-57.45	-38.63	-31.96	-21.82	-14.22
60	-42.84	-24.56	-20.27	-12.94	-6.88
30	-17.72	-12.99	-9.41	-5.67	-2.26
0.1	0	0	0	0	0

[a]11.22 mmol L^{-1}. [b]11.22 mmol L^{-1} (separately prepared solution from that used at 278 K)

Calculation of $\chi_M T$ by the Evans' method formula:

The Evans' method formula[3] (equation S1) is used to calculate the mass susceptibility, χ_g ($cm^3\ g^{-1}$) of a sample based on: Δf, the shift (Hz) of the CD_2HCN peak in the paramagnetic solution compared to the reference pure CD_2HCN; m, the concentration of the paramagnetic complex solution (g cm^{-3}); f, the spectrometer frequency (Hz); d_0 and d_s, the densities of the solvent and solution respectively (g cm^{-3}); χ_0, the mass susceptibility of the solvent in $cm^3\ g^{-1}$.

$$\chi_g = \frac{3\Delta f}{4\pi m f} + \chi_0 + \chi_0 \frac{d_0 - d_s}{m} \qquad \textbf{(S1)}$$

However, equation S1 can be simplified by taking an approximation that $d_s = d_0 + m$. This is reasonable because the solutions used were dilute[4, 5] (8.77 – 11.23 mmol L^{-1}). This approximation leads to the second and third terms in equation S1 cancelling out, giving equation S2 which was used in the present analysis.

$$\chi_g = \frac{3\Delta f}{4\pi m f} \qquad \textbf{(S2)}$$

Multiplying χ_g by the molecular mass (M in g mol^{-1}) of the complex gives χ_M, the molar susceptibility ($cm^3\ mol^{-1}$). χ_M is corrected for the diamagnetic contributions of each sample according to $\chi_M^{dia}(\text{sample}) = -0.5 \times M \times 10^{-6}\ cm^3\ mol^{-1}$.[6] Finally, multiplying by T gives the magnetic susceptibility, $\chi_M T$, in units of $cm^3\ K\ mol^{-1}$.

In the absence of an internal reference tube for the pure CD_3CN, Δf is indirectly determined by the summation of $\Delta\Delta f$(SCO) and Δf^0. Δf^0 is Δf at atmospheric pressure which is calculated via equation S3:

$$\Delta f^0 = \frac{4\pi m f}{3}\left(\frac{\chi_M T^0}{T \cdot M} - 0.5 \times 10^{-6}\right) \qquad \textbf{(S3)}$$

where $\chi_M T^0$ is the magnetic susceptibility in CD_3CN solution at atmospheric pressure of the complex at the particular temperature; these values are previously reported from our initial variable temperature solution SCO investigations of the $[Fe^{II}_2(\textbf{PSRT})_2](BF_4)_4$ complexes.[1] Parameter m is the concentration (g cm^{-3}) of the solution in the variable-pressure experiment and includes a correction for change in density of pure acetonitrile as a function of pressure and temperature (see below).

For each temperature, Δf^0 is determined for the solution concentration used and represents the shift (Hz) of the CD_2HCN peak in the paramagnetic solution compared to where the reference pure CD_2HCN would be if an internal reference tube was present in the high pressure cell.

Adding $\Delta\Delta f$(SCO) of each variable pressure spectrum (which are relative to the atmospheric pressure spectrum of that temperature) to Δf^0 of that temperature, gives Δf which is used to calculate $\chi_M T$ for that pressure point by equation S2. The $\chi_M T$ values 0.1-240 MPa and 278-313 K for the three Fe(II) complexes are presented in Tables S9-11.

The concentration of the paramagnetic solution, m (g cm^{-3}), is temperature and pressure dependent due to changes in the density of CD_3CN. Variable pressure density data for CH_3CN have been reported at 50 MPa increments up to 300 MPa at 283 and 313 K.[7] Fitting a cubic function to the reported data allows for the densities at the pressures used in this study (30 MPa increments up to 240 MPa) to be reliably approximated. Density vs pressure curves for the three other temperatures (278 K, 293 K, and 303 K) were approximated using the relative difference in density at atmospheric pressure to 283 K and 313 K data (Figure S6, Table S8).

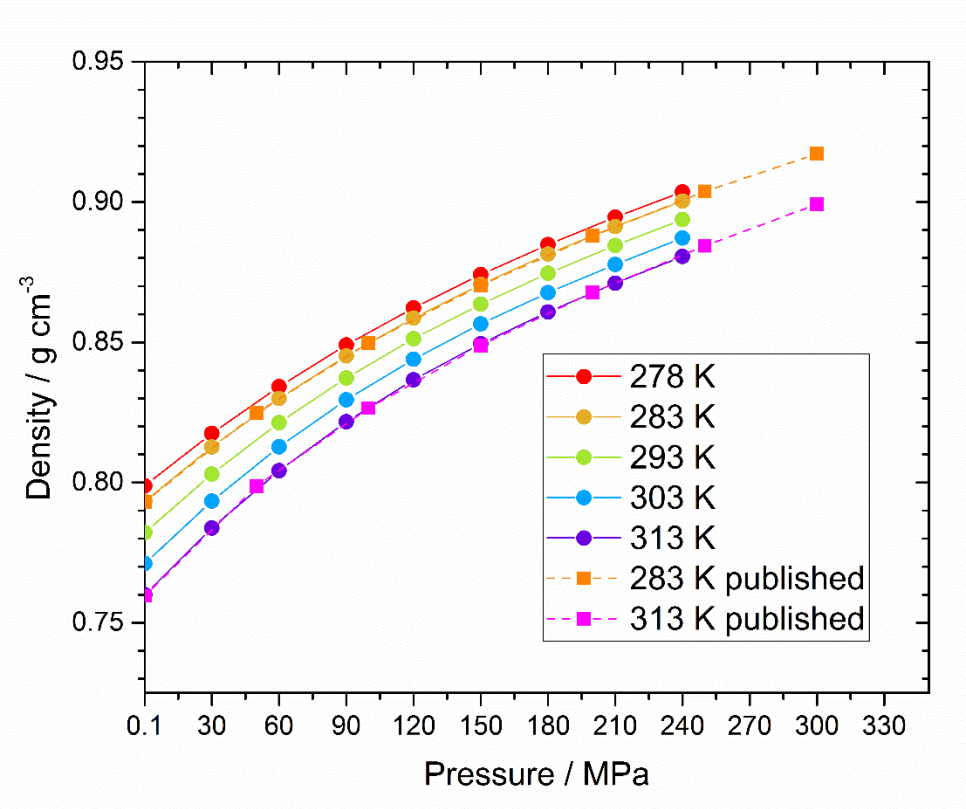

Figure S6. Approximated acetonitrile density vs pressure curves at 278, 283, 293, 303, and 313 K (circles, solid lines). The literature data reported at 283 K and 313 K are also shown (squares, dashed lines).[7] These data were used to correct the volumes (and hence concentrations) of the solutions of the Zn(II) and Fe(II) complexes for the effects of temperature and pressure.

Table S8. CD_3CN density values at various temperatures and pressures used in the calculation of *m* and subsequently, $\chi_M T$.

Pressure (MPa)	Density (g cm^{-3})				
	278 K	**283 K**	**293 K**	**303 K**	**313 K**
0.1	0.799	0.793	0.782	0.771	0.760
30	0.818	0.813	0.803	0.793	0.784
60	0.834	0.830	0.821	0.813	0.804
90	0.849	0.845	0.837	0.829	0.822
120	0.862	0.859	0.851	0.844	0.837
150	0.874	0.871	0.864	0.857	0.849
180	0.885	0.881	0.875	0.868	0.861
210	0.895	0.891	0.884	0.878	0.871
240	0.904	0.900	0.894	0.887	0.881

Table S9. $\chi_M T$ at various pressures and temperatures of $[Fe^{II}_2(\mathbf{PSPhT})_2](BF_4)_4 \cdot CH_3CN$ in CD_3CN solution.

Pressure (MPa)	$\chi_M T$ (cm^3 K mol^{-1})				
	278 K	283 K	293 K	303 K	313 K
240	3.62	3.99	4.16	4.54	4.86
210	3.77	4.17	4.36	4.70	5.02
180	3.92	4.33	4.54	4.88	5.20
150	4.06	4.50	4.73	5.08	5.39
120	4.21	4.68	4.92	5.27	5.57
90	4.45	4.86	5.12	5.47	5.76
60	4.73	5.06	5.32	5.67	5.95
30	4.97	5.26	5.54	5.88	6.14
0.1	5.22	5.46	5.76	6.10	6.34

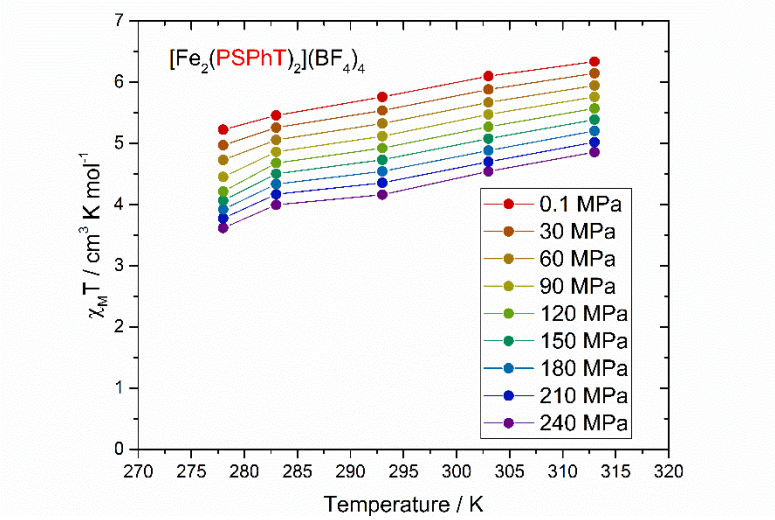

Figure S7. $\chi_M T$ vs. temperature at variable pressures for $[Fe^{II}_2(\mathbf{PSPhT})_2](BF_4)_4 \cdot CH_3CN$ in CD_3CN solution.

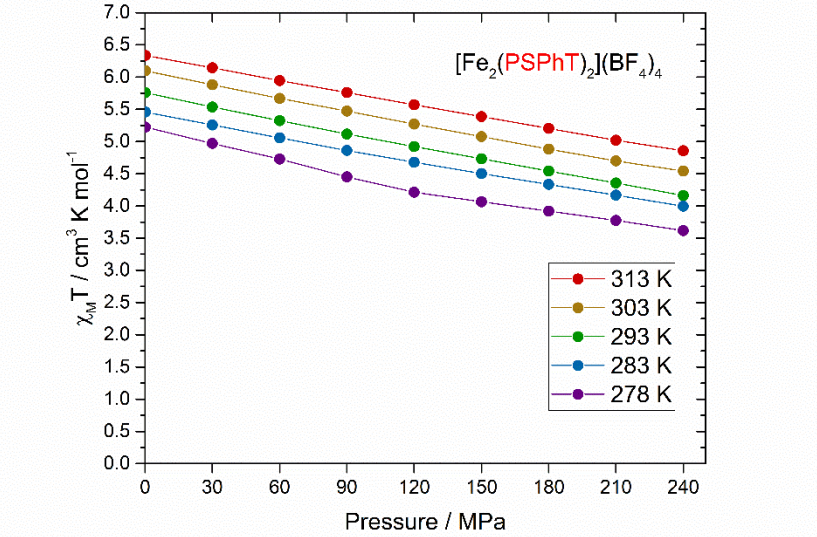

Figure S8. $\chi_M T$ vs. pressure at variable temperatures for $[Fe^{II}_2(\mathbf{PSPhT})_2](BF_4)_4 \cdot CH_3CN$ in CD_3CN solution.

Table S10. $\chi_M T$ at various pressures and temperatures of $[Fe^{II}_2(PS^{Me}PhT)_2](BF_4)_4$ in CD_3CN solution.

Pressure (MPa)	$\chi_M T$ (cm^3 K mol^{-1})				
	278 K	283 K	293 K	303 K	313 K
240	2.94	3.26	3.51	3.83	4.08
210	3.10	3.41	3.68	3.99	4.27
180	3.23	3.58	3.86	4.17	4.44
150	3.38	3.76	4.03	4.34	4.61
120	3.52	3.94	4.21	4.53	4.79
90	3.68	4.14	4.39	4.71	4.96
60	4.01	4.32	4.58	4.90	5.13
30	4.29	4.53	4.78	5.09	5.32
0.1	4.53	4.75	5.00	5.28	5.50

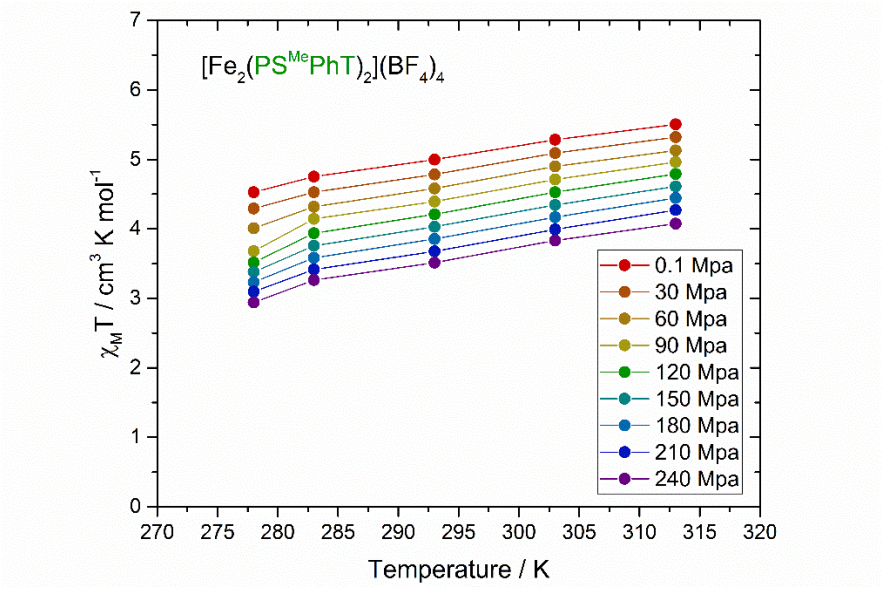

Figure 9. $\chi_M T$ vs. temperature at variable pressures for $[Fe^{II}_2(PS^{Me}PhT)_2](BF_4)_4$ in CD_3CN solution.

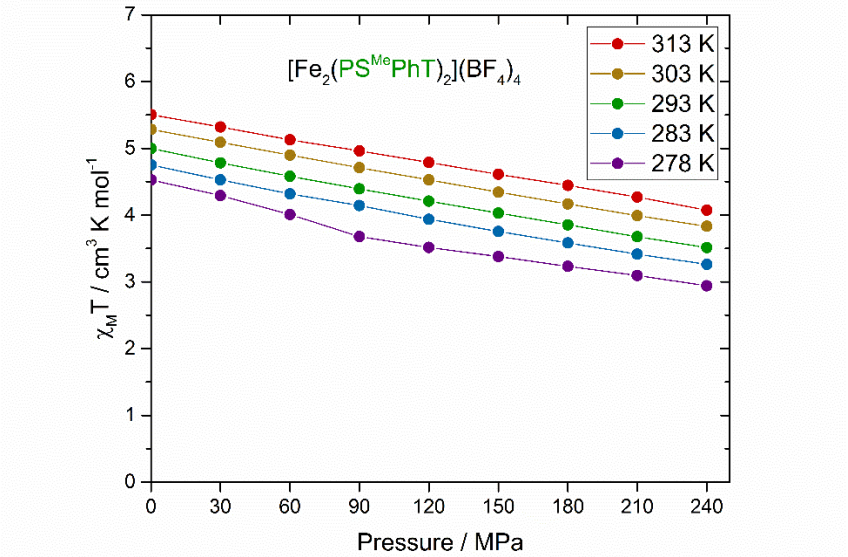

Figure S10. $\chi_M T$ vs. pressure at variable temperatures for $[Fe^{II}_2(PS^{Me}PhT)_2](BF_4)_4$ in CD_3CN solution.

Table S11. $\chi_M T$ at various pressures and temperatures of $[Fe^{II}_2(PS^{i}BuT)_2](BF_4)_4 \cdot \frac{1}{2}H_2O$ in CD_3CN solution.

Pressure (MPa)	$\chi_M T$ (cm^3 K mol^{-1})				
	278 K	283 K	293 K	303 K	313 K
240	1.69	2.00	2.37	2.80	3.15
210	1.85	2.20	2.58	3.01	3.36
180	2.03	2.39	2.79	3.20	3.55
150	2.21	2.58	2.99	3.40	3.73
120	2.41	2.77	3.19	3.60	3.91
90	2.59	2.98	3.38	3.79	4.08
60	2.79	3.19	3.58	3.97	4.26
30	3.13	3.39	3.79	4.16	4.43
0.1	3.40	3.62	4.00	4.35	4.59

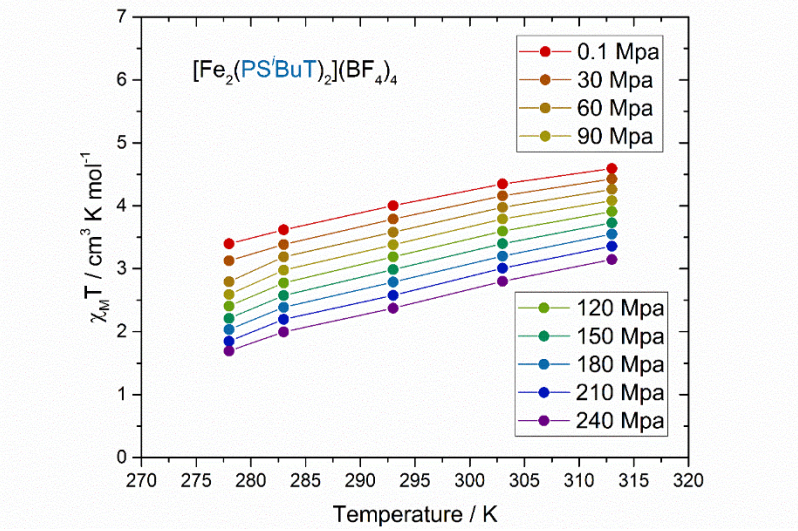

Figure S11. $\chi_M T$ vs. temperature at variable pressures for $[Fe^{II}_2(PS^{i}BuT)_2](BF_4)_4 \cdot \frac{1}{2}H_2O$ in CD_3CN solution.

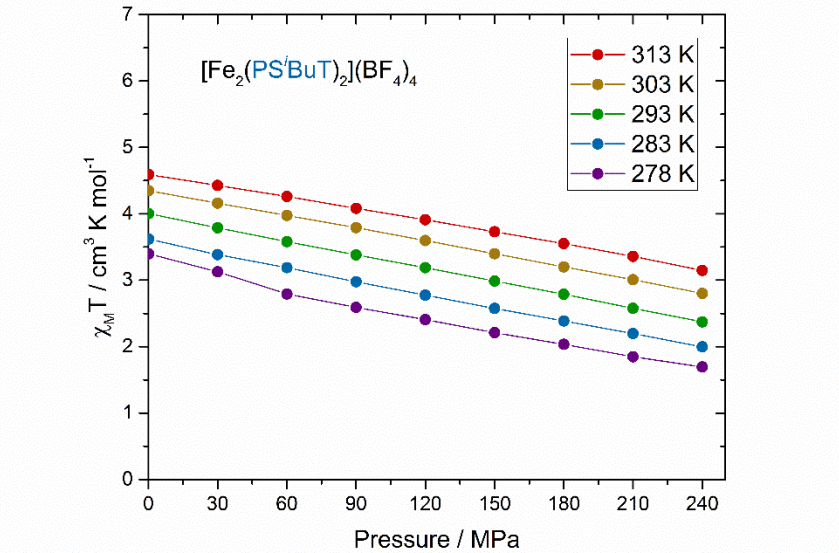

Figure S12. $\chi_M T$ vs. pressure at variable temperatures for $[Fe^{II}_2(PS^{i}BuT)_2](BF_4)_4 \cdot \frac{1}{2}H_2O$ in CD_3CN solution.

Determination of error in calculated $\chi_M T$ by analysis of proton chemical shifts

By analysis of line widths in the ^{1}H NMR spectra and distance of protons in the ligand scaffold from the paramagnetic Fe(II) centres, the signals were tentatively assigned for [Fe$^{II}_2$(**PSPhT**)$_2$](BF$_4$)$_4$·CH$_3$CN (Figure S13). As the pyridine moiety features in all three complexes, these proton signals are found at similar chemical shifts in each of the three complexes. Protons py-H4 and py-H5 were chosen in the analysis of the relationship between isotropic chemical shift, δ_{iso} (the shift relative to the chemical shift in the diamagnetic state), and the calculated magnetic susceptibilities, $\chi_M T$.

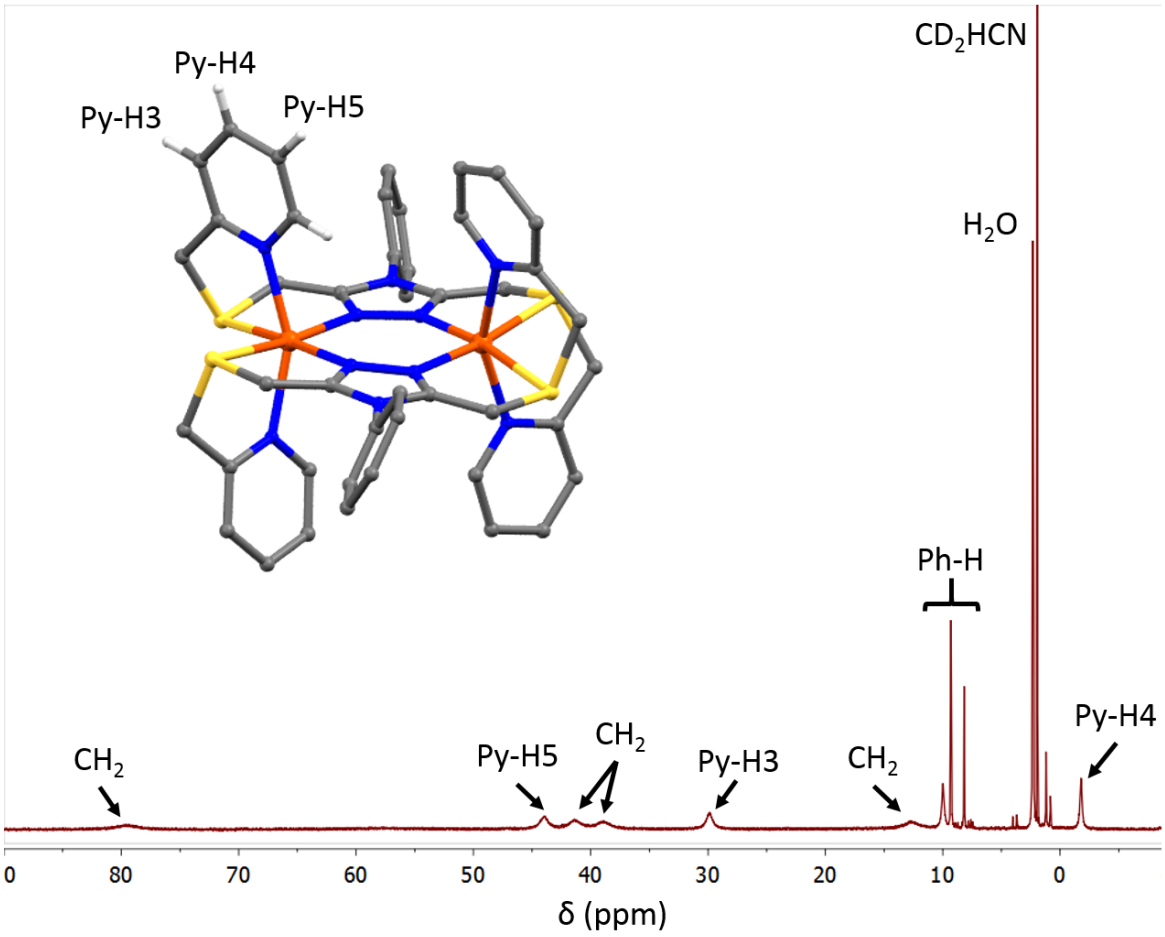

Figure S13. ^{1}H NMR spectrum of [Fe$^{II}_2$(**PSPhT**)$_2$](BF$_4$)$_4$·CH$_3$CN in CD$_3$CN at 240 MPa, 293 K, with tentative assignments.

Assuming an ideal Curie behaviour of the chemical shifts and ignoring the possibility of ring currents affecting diamagnetic behaviour,[8] $\delta_{iso} \times T$ should correlate linearly with $\chi_M T$,[9, 10] and therefore δ_{iso} linearly with χ_M. For this analysis, we are only interested in the linear relationship between chemical shift and χ_M and hence the slope of δ_{iso} vs χ_M. The diamagnetic chemical shift correction, δ_{LS} applied to that observed in the Fe(II) spectra, δ, to obtain δ_{iso} affects only the y-intercept of any δ_{iso} vs χ_M plot. The data presented here is of the absolute chemical shift of the signals assigned to py-H4 and py-H5, $\delta_{py\text{-}H4}$ and $\delta_{py\text{-}H5}$ (Figures S14-S19). As all spectra were recorded with no lock on the solvent CD$_2$HCN signal, for the purposes of analysing the proton chemical shifts, the CD$_2$HCN signal was manually referenced to 1.94 ppm.

For each Fe(II) complex, variable pressure data at 278 K were recorded for a separately prepared solution to that used for data at 278-313 K. For the $\delta_{py\text{-}H4}/\delta_{py\text{-}H5}$ vs χ_M plots, 278 K data is treated as a separate data series to 283-313 K data, and a linear fit is applied to each data series. This allows for the error analysis of $\chi_M T$ to be separated into two sources of error: that associated with solution preparation, error A (error between 278 K and 283-313 K data series); and that associated with $\chi_M T$ calculated on the same solution (error within each 278 K series and 283-313 K series) which reflects the error in the extra corrections required for this adapted Evans' method. For each $\delta_{py\text{-}H4}/\delta_{py\text{-}H5}$ vs χ_M plot, the data point from the 278 K series which sits furthest on the x-axis from the linear fit of 283-313 K is indicated with the percentage difference in χ_M from that linear fit; this represents error A. The data point in each of the 278 K and 283-313 K series that sits furthest on the *x*-axis from its respective linear fit is indicated with the percentage difference in χ_M; these represent error B. Estimated errors are summarized in Table S12.

Table S12. Estimated error in the calculated χ_M, and hence $\chi_M T$ values as determined by analysis of the Fe(II) complex proton chemical shift data. Error A is the maximum disagreement between 278 K data and 283-313 K data. Error B is the maximum disagreement within either the 278 K or 283-313 K data series.

Complex	Error A	Error B
$[Fe^{II}_2(\mathbf{PSPhT})_2](BF_4)_4{\cdot}CH_3CN$	7.4%	3.0%
$[Fe^{II}_2(\mathbf{PS^{Me}PhT})_2](BF_4)_4$	8.7%	5.2%
$[Fe^{II}_2(\mathbf{PS^{i}BuT})_2](BF_4)_4{\cdot}½H_2O$	6.2 %	3.2%

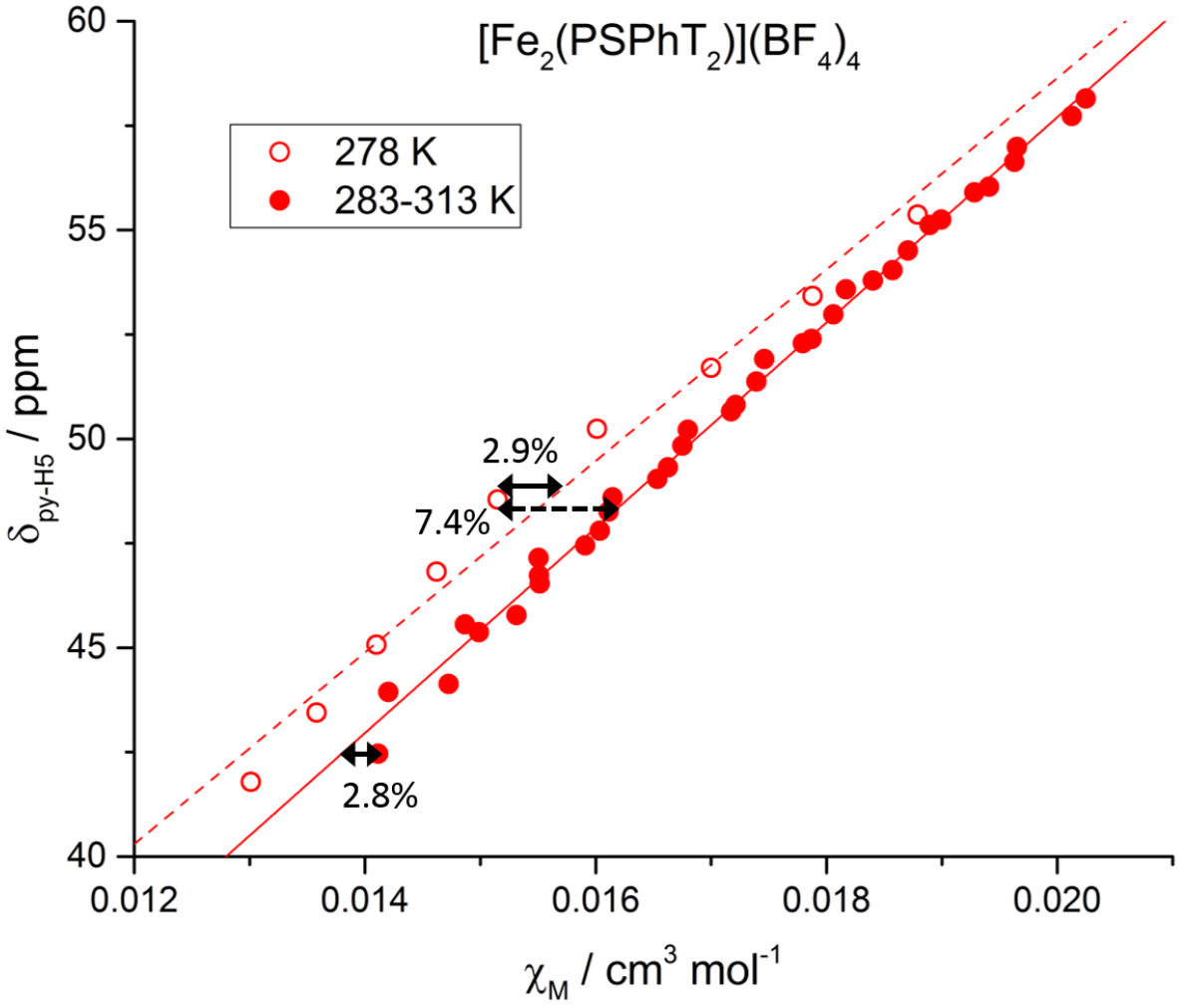

Figure S14. $\delta_{py\text{-}H5}$ vs χ_M for $[Fe^{II}_2(\mathbf{PSPhT})_2](BF_4)_4$ in CD_3CN at variable pressure/temperature. Hollow data points represent spectra recorded at 278 K, with linear fit shown by the dashed line. Solid data points recorded at 283-313 K, with solid line for linear fit.

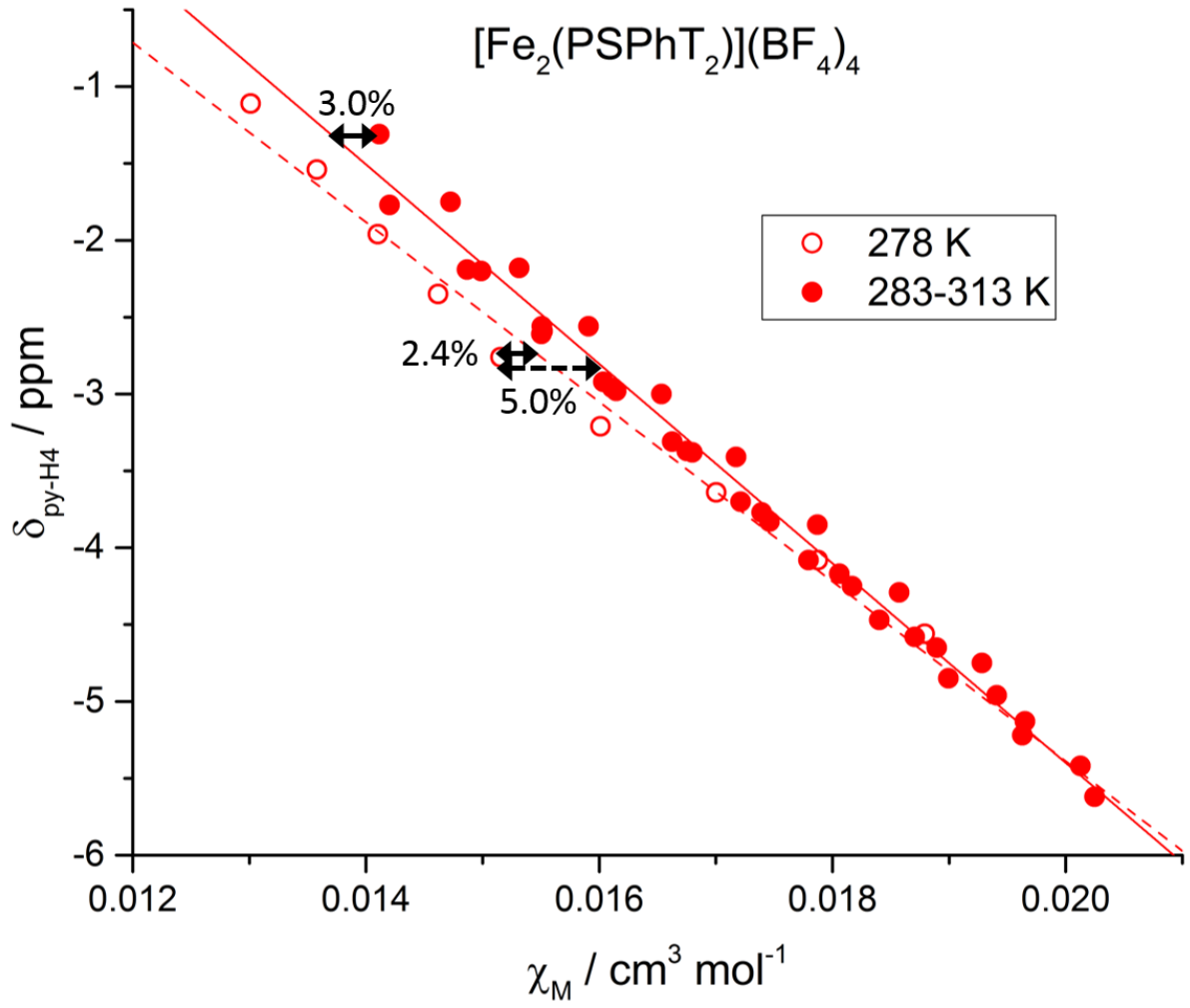

Figure S15. $\delta_{py\text{-}H4}$ vs χ_M for $[Fe^{II}_2(\mathbf{PSPhT})_2](BF_4)_4$ in CD_3CN at variable pressure/temperature. Hollow data points represent spectra recorded at 278 K, with linear fit shown by the dashed line. Solid data points recorded at 283-313 K, with solid line for linear fit.

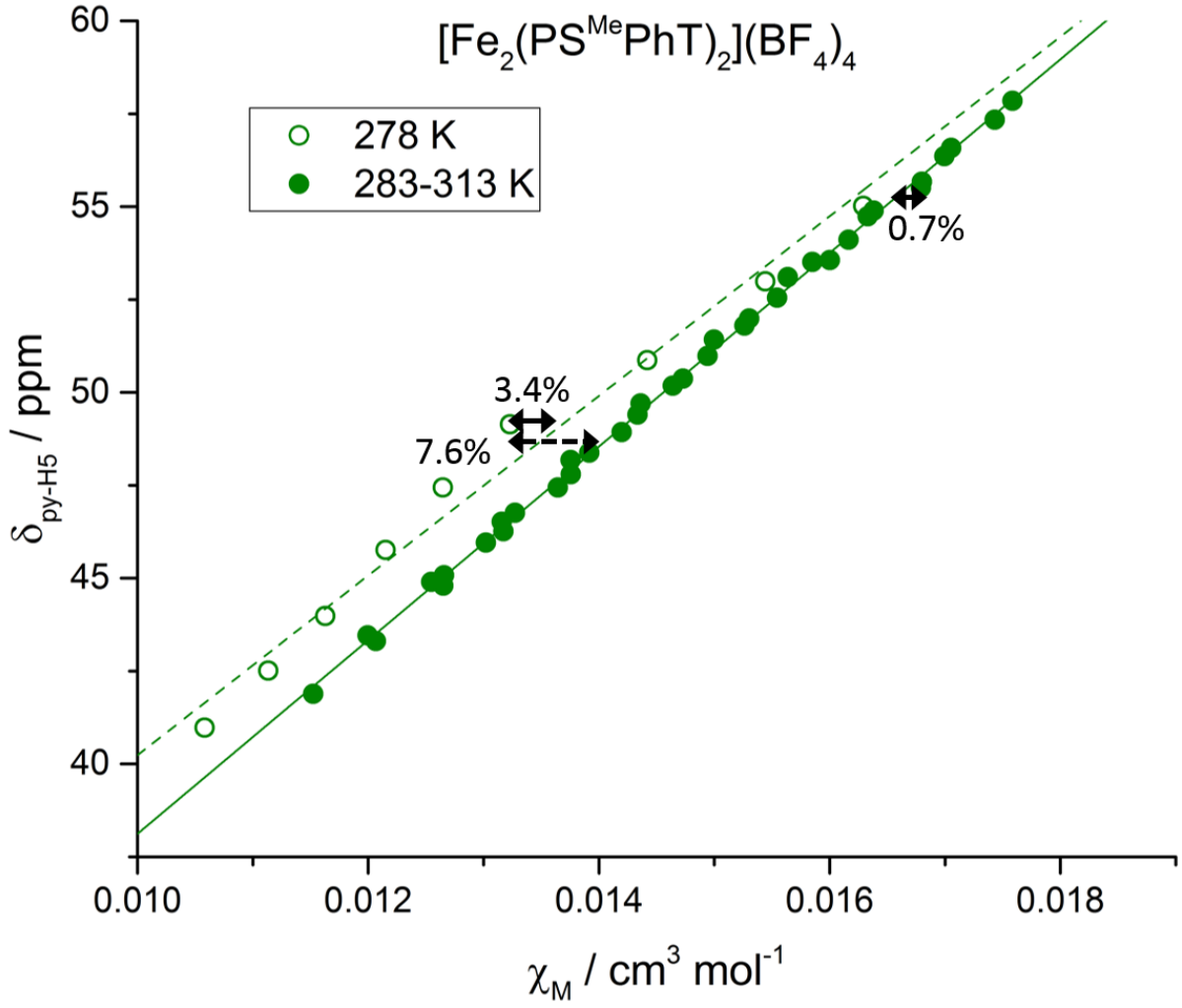

Figure S16. $\delta_{py\text{-}H5}$ vs χ_M for $[Fe^{II}_2(PS^{Me}PhT)_2](BF_4)_4$ in CD_3CN at variable pressure/temperature. Hollow data points represent spectra recorded at 278 K, with linear fit shown by the dashed line. Solid data points recorded at 283-313 K, with solid line for linear fit.

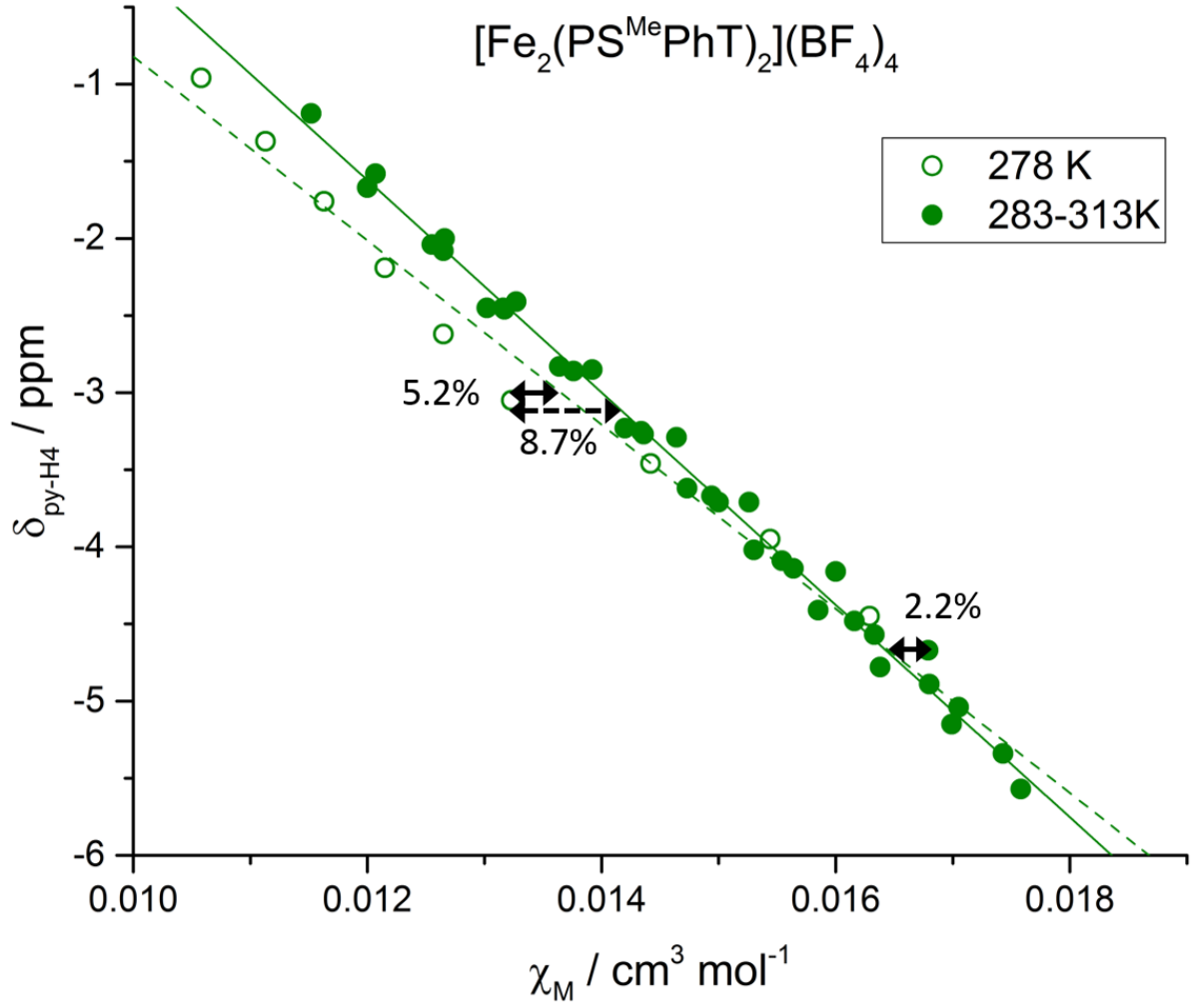

Figure S17. $\delta_{py\text{-}H4}$ vs χ_M for $[Fe^{II}_2(PS^{Me}PhT)_2](BF_4)_4$ in CD_3CN at variable pressure/temperature. Hollow data points represent spectra recorded at 278 K, with linear fit shown by the dashed line. Solid data points recorded at 283-313 K, with solid line for linear fit.

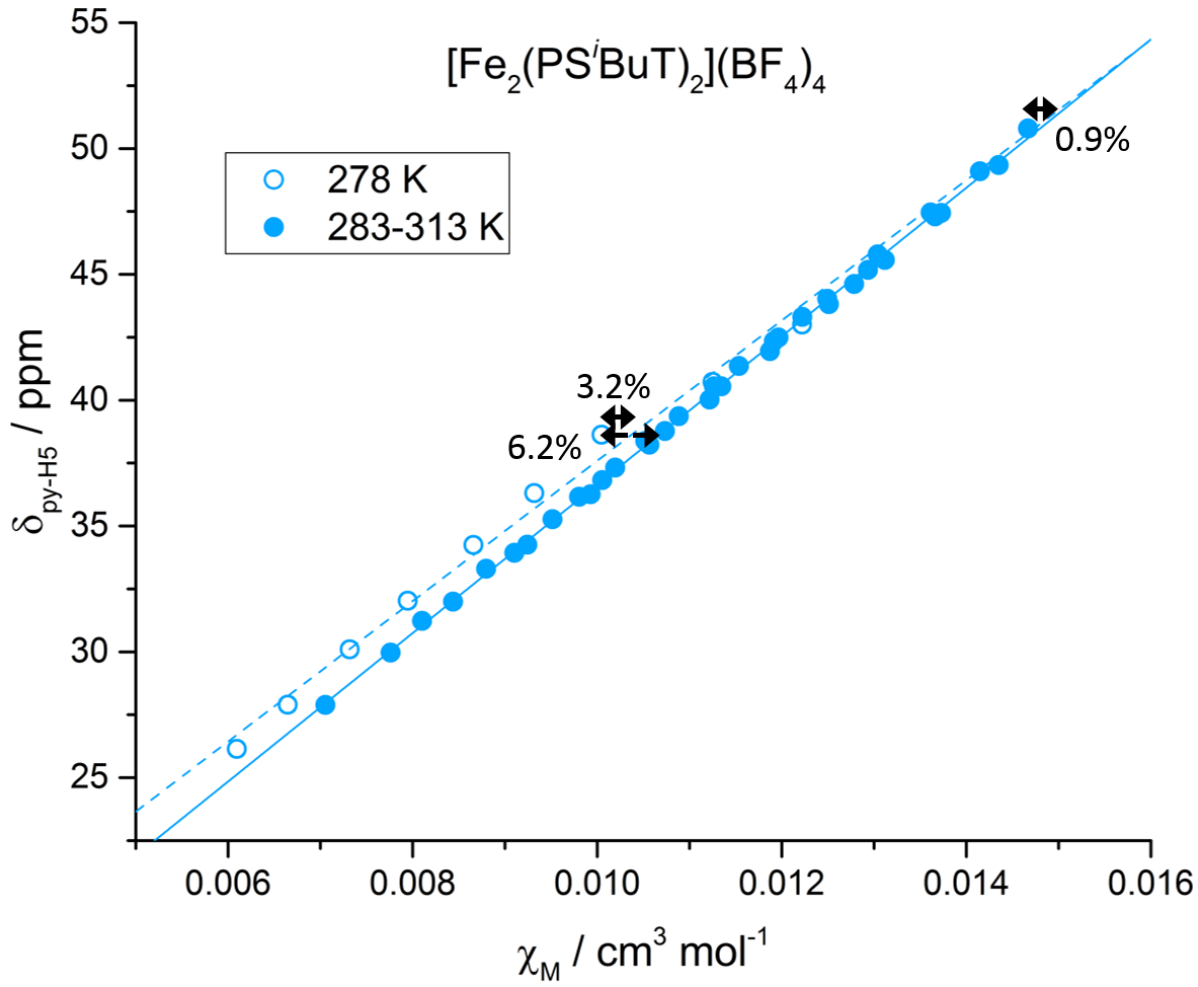

Figure S18. $\delta_{py\text{-}H5}$ vs χ_M for [Fe^{II}_2(**PS^{i}BuT**)$_2$](BF$_4$)$_4$ in CD_3CN at variable pressure/temperature. Hollow data points represent spectra recorded at 278 K, with linear fit shown by the dashed line. Solid data points recorded at 283-313 K, with solid line for linear fit.

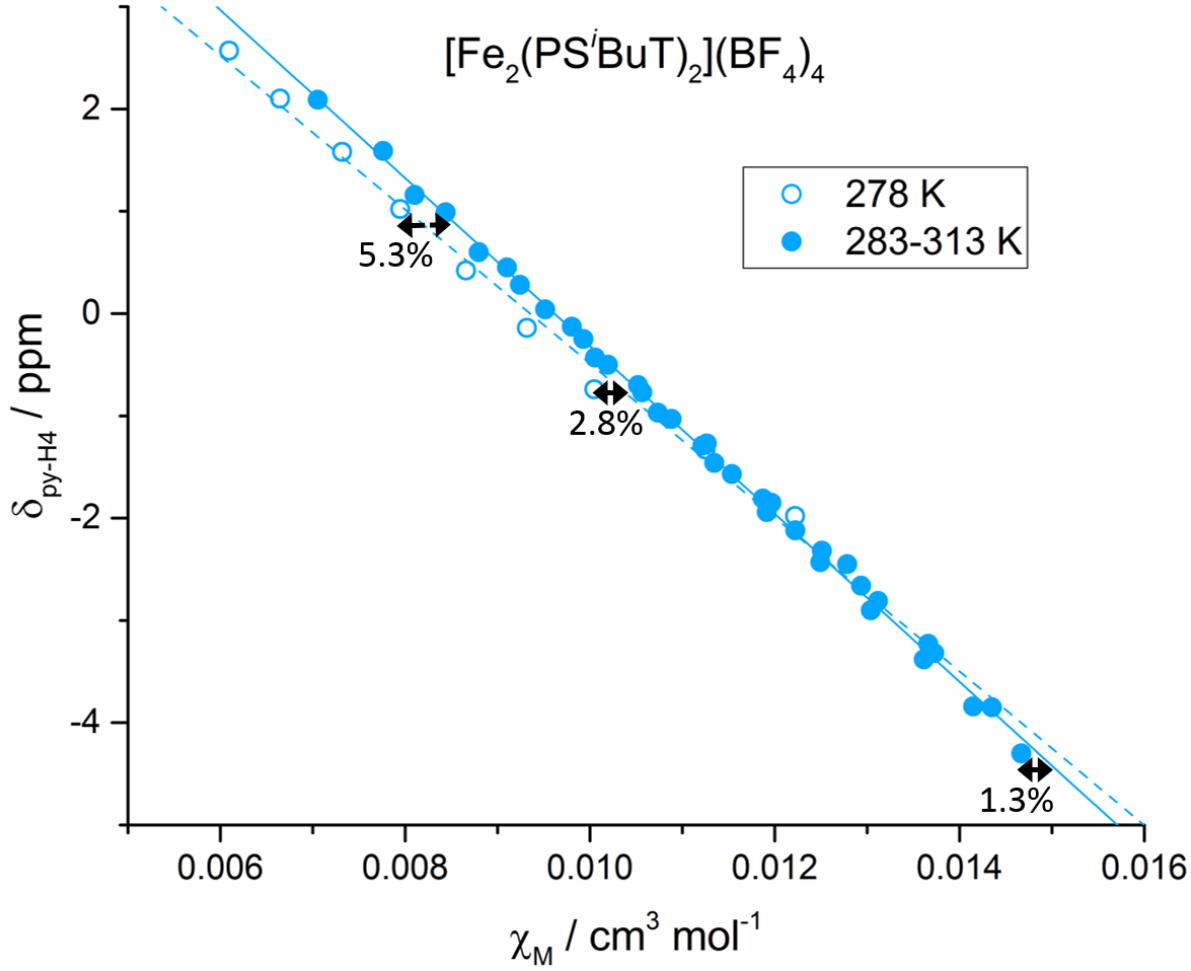

Figure S19. $\delta_{py\text{-}H4}$ vs χ_M for [Fe^{II}_2(**PS^{i}BuT**)$_2$](BF$_4$)$_4$ in CD_3CN at variable pressure/temperature. Hollow data points represent spectra recorded at 278 K, with linear fit shown by the dashed line. Solid data points recorded at 283-313 K, with solid line for linear fit.

X-ray crystal structure of [Zn_2(PSPhT)$_2$](BF$_4$)$_4$·2MeCN

X-Ray crystallographic data were collected on an Oxford Diffraction SuperNova diffractometer with Atlas CCD, equipped with a Cryostream N_2 open-flow cooling device, using mirror monochromated micro-focus Cu-Kα radiation at 100 K. Scans were performed in such a way as to collect a complete set of unique reflections to a maximum resolution of 0.80 Å. Raw frame data (including data reduction, inter-frame scaling, unit cell refinement and absorption corrections) for all structures were processed using *CrysAlis Pro*[11] Structures were solved using *SUPERFLIP*[12] and refined against all F^2 data using *SHELXL-2014*.[13] Hydrogen atoms were inserted at calculated positions with U(H) = 1.2 U(attached atom), and rode on the atoms to which they were attached. All non-H atoms were refined with anisotropic thermal parameters. The thermal ellipsoids of both of the half-occupancy solvent MeCN molecule were restrained using the SIMU command. High resolution pictures were prepared using Mercury[14] and POVray[15] software. CCDC 1554635.

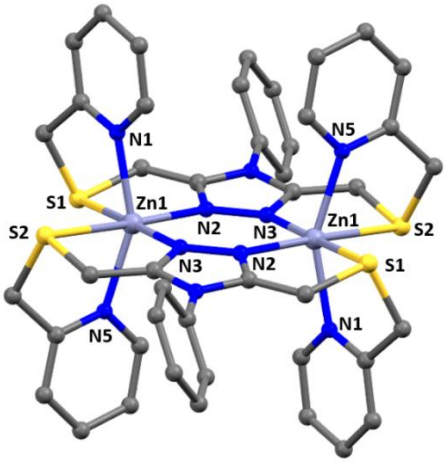

Figure S20. Perspective view of the cation of $[Zn_2(\mathbf{PSPhT})_2](BF_4)_4{\cdot}2MeCN$. Note that the **PSPhT** ligands are coordinated in the cis-axial mode with an inversion centre between the two iron centres. Colour codes: zinc, indigo; nitrogen, royal blue; sulfur, yellow; carbon, grey. Hydrogen atoms omitted.

Table S12 Crystal data and structure refinement details for $[Zn_2(\mathbf{PSPhT})_2](BF_4)_4{\cdot}2MeCN$

	$[Zn_2(\mathbf{PSPhT})_2](BF_4)_4{\cdot}2MeCN$
Empirical formula	$C_{48}H_{48}B_4F_{16}N_{12}S_4Zn_2$
Mr	1399.20
Crystal system	triclinic
Space group	$P\overline{1}$
***a* [Å]**	9.9090(4)
***b* [Å]**	12.3948(6)
***c* [Å]**	14.9001(4)
***α* [°]**	101.753(3)
***β* [°]**	96.938(3)
***γ* [°]**	111.945(4)
***V* [Å^3]**	1622.32(11)
Z	1
***T* [K]**	100(2)
$\rho_{calcd.}$ **[g/cm^3]**	1.432
μ **[mm^{-1}]**	2.898
***F*(000)**	708
Crystal Size (mm)	0.19 x 0.08 x 0.07
θ range for data collection	3.994 to 76.473
Reflections collected	19929
Independent reflections	6718
***R*(int)**	0.0515
Max. and min. transmission	1.0 and 0.71319
Data / restraints / parameters	6718 / 24 / 417
Goof (F^2)	1.162
R_1 **[I>2σ(I)]**	0.0885
wR_2 **[all data]**	0.2659
Max/min res. e density [eÅ^{-3}]	2.079 and -1.434

^{1}H NMR Spectra of the Diamagnetic Zn(II) reference solutions

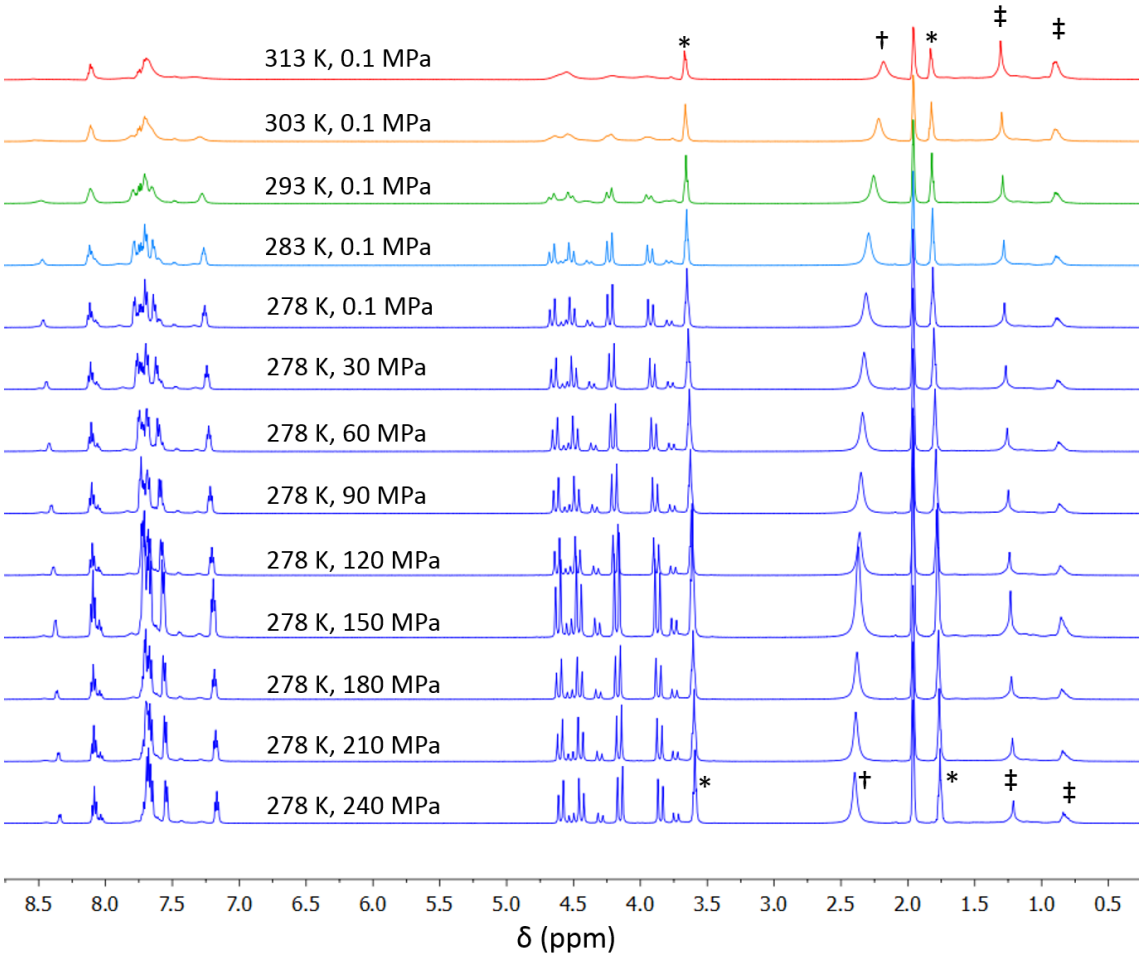

Figure S21. ^{1}H NMR spectra of $[Zn^{II}_2(\mathbf{PSPhT})_2](BF_4)_4 \cdot 1½THF$ in CD_3CN from 313 K to 278 K at atmospheric pressure, and from atmospheric pressure to 240 MPa at 278 K. Note: * indicates residual THF, † indicates H_2O, ‡ indicates paraffin oil.

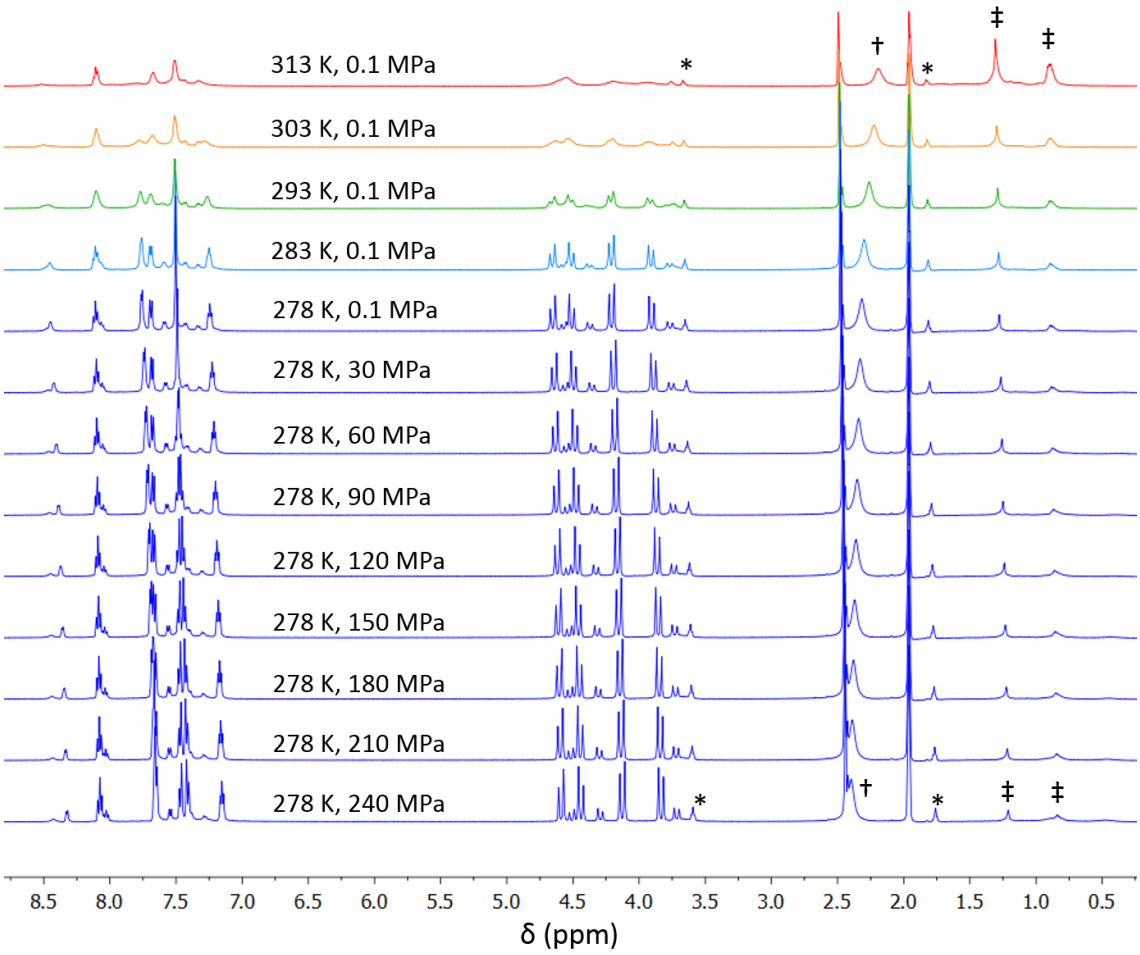

Figure S22. ^{1}H NMR spectra of $[Zn^{II}_2(\mathbf{PS^{Me}PhT})_2](BF_4)_4 \cdot \frac{1}{3}THF$ in CD_3CN from 313 K to 278 K at atmospheric pressure, and from atmospheric pressure to 240 MPa at 278 K. Note: * indicates residual THF, † indicates H_2O, ‡ indicates paraffin oil.

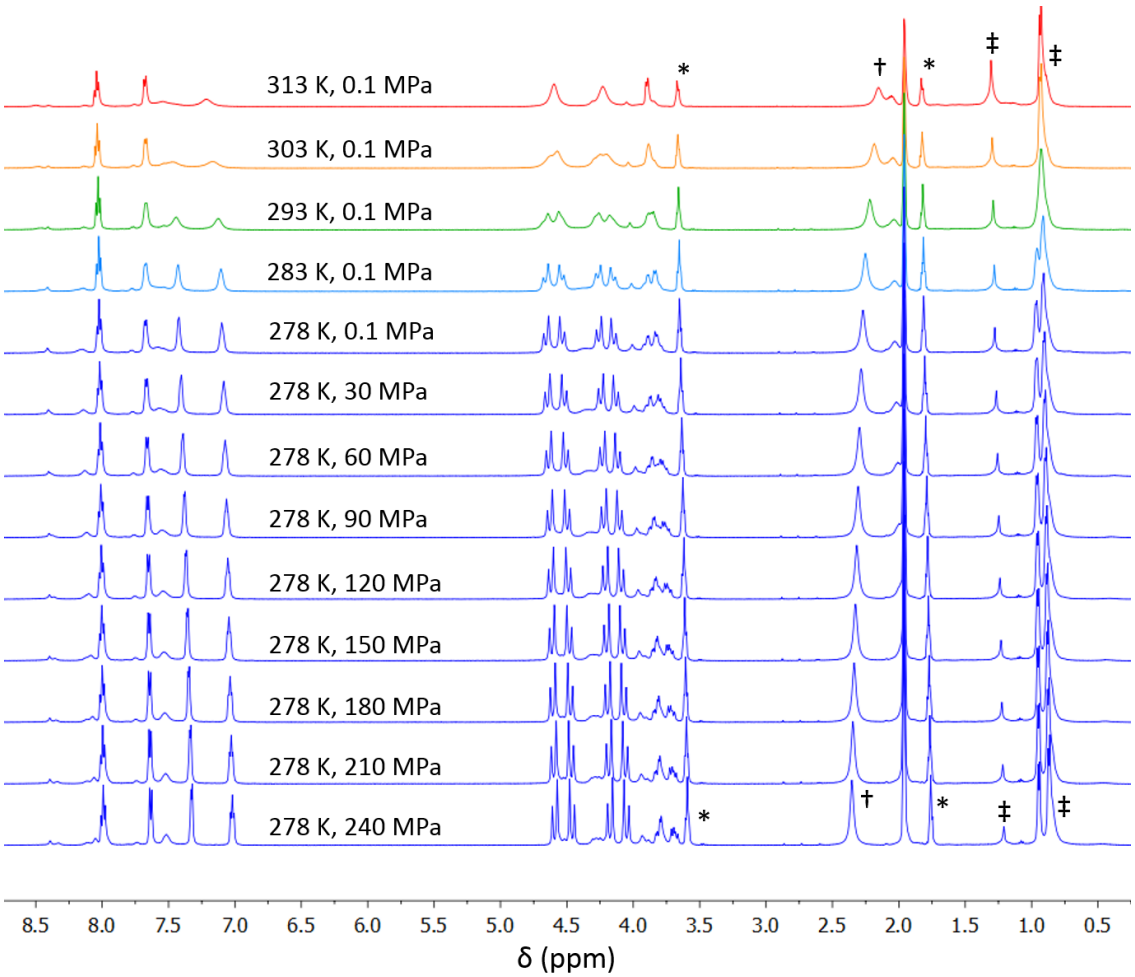

Figure S23. ^{1}H NMR spectra of [Zn^{II}_{2}(**PS^{i}BuT**)$_2$](BF$_4$)$_4$·THF in CD_3CN from 313 K to 278 K at atmospheric pressure, and from atmospheric pressure to 240 MPa at 278 K. Note: * indicates residual THF, † indicates H_2O, ‡ indicates paraffin oil.

References

1. R. W. Hogue, H. L. C. Feltham, R. G. Miller and S. Brooker, *Inorg. Chem.*, 2016, **55**, 4152–4165.
2. C. P. Lepper, M. A. K. Williams, P. J. B. Edwards and G. B. Jameson, *Chem. N. Z.*, 2014, **78**, 122-125.
3. D. F. Evans, *J. Chem. Soc.*, 1959, 2003-2005.
4. J. W. Turner and F. A. Schultz, *Inorg. Chem.*, 2001, **40**, 5296-5298.
5. C. Piguet, *J. Chem. Ed.*, 1997, **74**, 815-816.
6. O. Kahn, *Molecular Magnetism*, VCH Publishers Inc., New York, 1993.
7. K. R. Srinivasan and R. L. Kay, *J. Solution Chem.*, 1977, **6**, 357-367.
8. M. Kozik, N. Casan-Pastor, C. F. Hammer and L. C. W. Baker, *J. Am. Chem. Soc.*, 1988, **110**, 7697-7701.
9. B. Weber and F. A. Walker, *Inorg. Chem.*, 2007, **46**, 6794-6803.
10. H. Petzold, P. Djomgoue, G. Horner, J. M. Speck, T. Ruffer and D. Schaarschmidt, *Dalton Trans.*, 2016, **45**, 13798-13809.
11. *CrysAlisPro*, Version 171.37.33; Agilent Technologies Yarnton, Oxfordshire, 2014.
12. L. Palatinus and G. Chapuis, *J. Appl. Crystallogr.*, 2007, **40**, 786-790.
13. G. Sheldrick, *Acta Crystallogr., Sect. C*, 2015, **71**, 3-8.
14. C. F. Macrae, I. J. Bruno, J. A. Chisholm, P. R. Edgington, P. McCabe, E. Pidcock, L. Rodriguez-Monge, R. Taylor, J. van de Streek and P. A. Wood, *J. Appl. Crystallogr.*, 2008, **41**, 466-470.
15. *POVray Persistence of Vision Raytracer*, Version 3.7; Persistence of Vision Pty. Ltd.: 2013.